Performance of improved high-order filter schemes for turbulent flows with shocks

By D. Kotov, H.C. Yee AND B. Sjögreen

1. Motivation and Objectives

In simulations of multiscale compressible turbulent flows with discontinuities, the constructions of numerical schemes for stable and accurate simulation of shock/turbulence interaction share one important ingredient - minimization of numerical dissipation while maintaining numerical stability. Methods commonly used for these simulations rely on switching between spectral or high-order compact schemes to shock-capturing schemes and are not always practical for multiscale shock/turbulence interactions. Also frequent switching between these two types of schemes can create severe numerical instability. One possible way of overcoming these difficulties is by using high-order nonlinear filter schemes (Yee & Sjögreen 2007, 2009; Sjögreen & Yee 2004). These schemes take advantage of the effectiveness of the nonlinear dissipation contained in good shock-capturing schemes as stabilizing mechanisms at locations where needed. In addition to the minimization of numerical dissipation while maintaining numerical stability in compressible turbulence with strong shock, Yee & Sjögreen (2002), Yee (2002), Yee & Sweby (1997) and Yee *et al.* (1999) discussed a general framework for the design of such schemes.

One of the key parameters responsible for minimizing numerical dissipation in nonlinear filter schemes is the numerical dissipation control parameter κ. In the original version of filter schemes this parameter required some tuning based on the knowledge of the flow physics for the particular case. The technique considered in this study made use of a flow location dependence κ as a function of the local Mach number M in such way that the scheme would be suitable for a wide range of flow types without additional tuning. The basic idea of developing a local flow sensor with improved control on numerical dissipation that is inherited in the chosen shock-capturing scheme was proposed in Yee & Sjögreen (2009). In particular, a local Mach sensor $\kappa(M)$ was proposed by Yee & Sjögreen without extensive numerical experiments. This is a sequel study of Yee & Sjögreen (2009) with comparative evaluation for the same test cases as in Johnsen *et al.* (2010) to illustrate the performance of the local Mach sensor. The results obtained using constant κ based on the free stream Mach number have been presented in Johnsen *et al.* (2010). This study addresses the same problems as in Johnsen *et al.* (2010) and compares the results obtained using $\kappa = \text{const}$ with the new results obtained by applying global or local κ numerical dissipation control.

2. Improved High-Order Filter Schemes

2.1. *Original High-Order Filter Scheme*

Consider the 3-D compressible Euler equations in Cartesian geometry,

$$U_t + \nabla \cdot \mathbf{F} = \mathbf{0};\; U = \begin{pmatrix} \rho \\ \rho\mathbf{u} \\ e \end{pmatrix};\; \mathbf{F} = \begin{pmatrix} \rho\mathbf{u} \\ \rho\mathbf{u}\mathbf{u}^T + p \\ \mathbf{u}(e+p) \end{pmatrix}. \tag{2.1}$$

Here the velocity vector $\mathbf{u} = (u, v, w)^T$, ρ is the density, e is the total energy, and p is the pressure.

The high-order nonlinear filter scheme of Yee & Sjögreen (2007) when used to solve the fully coupled system (2.1), consists of three steps.

2.1.1. *Preprocessing Step*

Before the application of a high-order non-dissipative spatial base scheme, a preprocessing step is employed to improve the stability. The inviscid flux derivatives of the governing equation(s) are split in the following three ways, depending on the flow types and the desire for rigorous mathematical analysis or physical argument.

- Entropy splitting of Olsson & Oliger (1994) and Yee *et al.* (2000); Yee & Sjögreen (2002). The resulting form is non-conservative and the derivation is based on entropy norm stability with boundary closure for the initial value boundary problem.
- The system form of the Ducros *et al.* (2000) splitting. This is a conservative splitting and the derivation is based on physical arguments.
- Tadmor entropy conservation formulation for systems Sjögreen & Yee (2009). The derivation is based on mathematical analysis. It is a generalization of Tadmor's entropy formulation to systems and has not been fully tested on complex flows.

2.1.2. *Base Scheme Step*

A full time step is advanced using a high-order non-dissipative (or very low dissipation) spatially central scheme on the split form of the governing partial differential equations (PDEs). Summation-by-parts (SBP) boundary operator (Olsson 1995; Sjögreen & Yee 2007) and matching order conservative high-order free stream metric evaluation for curvilinear grids (Vinokur & Yee 2002) are used. High-order temporal discretization such as the third-order or fourth-order Runge-Kutta (RK3 or RK4) method is used. It is remarked that other temporal discretizations can be used for the base scheme step.

2.1.3. *Post-Processing (Nonlinear Filter Step)*

To further improve nonlinear stability from the non-dissipative spatial base scheme, after the application of a non-dissipative high-order spatial base scheme on the split form of the governing equation(s) the post-processing step is used to nonlinearly filter the solution by a dissipative portion of a high-order shock-capturing scheme with a local flow sensor. The flow sensor provides locations and amounts of built-in shock-capturing dissipation that can be further reduced or eliminated. At each grid point, a local flow sensor, e.g., a multi-resolution wavelet, would be employed to analyze the regularity of the computed flow data. Only the discontinuity locations would receive the full amount of shock-capturing dissipation. In smooth regions, no shock-capturing dissipation would be added. In regions with strong turbulence, a small fraction of the shock-capturing dissipation would be added to improve stability. The nonlinear dissipative portion of a high-resolution shock-capturing scheme can be any shock-capturing scheme.

Let U^* be the solution after the completion of the base scheme step. The final update of the solution after the filter step is (with the numerical fluxes in the y- and z-directions suppressed as well as their corresponding y- and z-directions indices on the x inviscid flux suppressed)

$$U^{n+1}_{j,k,l} = U^*_{j,k,l} - \frac{\Delta t}{\Delta x}[H^*_{j+1/2} - H^*_{j-1/2}], \quad H_{j+1/2} = R_{j+1/2}\overline{H}_{j+1/2}, \tag{2.2}$$

where $R_{j+1/2}$ is the matrix of right eigenvectors of the Jacobian of the inviscid flux vector

in terms of the Roe's average states based on U^*. $H^*_{j+1/2}$ and $H^*_{j-1/2}$ are numerical fluxes in terms of the Roe's average states based on U^*. Denote the elements of the vector $\overline{H}_{j+1/2}$ by $\overline{h}^l_{j+1/2}, l = 1, 2, ..., 5$. The nonlinear portion of the filter $\overline{h}^l_{j+1/2}$ has the form

$$\overline{h}^l_{j+1/2} = \frac{\kappa}{2}\omega^l_{j+1/2}\phi^l_{j+1/2}. \tag{2.3}$$

Here $\omega^l_{j+1/2}$ is the wavelet flow sensor to activate the nonlinear numerical dissipation $\frac{1}{2}\phi^l_{j+1/2}$, and the original formulation for κ is a positive parameter that is less than or equal to one. The choice of the parameter κ can be different for different flow types. In the next section the local and the global implementation of κ is discussed. These techniques of choosing κ can be used to avoid tuning scheme parameters for a wide range of flows.

2.2. *An efficient global κ for low Mach number and smooth flows*

To overcome the shortcomings of the low speed Roe scheme, the flow speed indicator formula of Li & Gu (2008) was modified to obtain an improved global κ denoted by $\overline{\kappa}$ for Eq. (2.3) to minimize the tuning of the original κ for low Mach number flows. $\overline{\kappa}$ has the form

$$\overline{\kappa} = f_1(M)\kappa, \tag{2.4}$$

with

$$f_1(M) = \min\left(\frac{M^2}{2}\frac{\sqrt{4+(1-M^2)^2}}{1+M^2}, 1\right). \tag{2.5}$$

Here M is the maximum Mach number of the entire computational domain at each stage of the time evolution. $f_1(M)$ has the same form as in Li & Gu (2008) except for the extra factor $M/2$ added to the first argument on the right-hand-side of the original form $f(M)$ in equation (18) of Li & Gu (2008). The added factor provides a similar value of the tuning κ observed from numerical experimentation reported in the aforementioned works. With the flow speed indicator $f_1(M)$ in front of κ, the same κ used for the supersonic shock problem can be used without any tuning for the very low speed turbulent flow cases. Another minor modification of the above is

$$\overline{f_1(M)} = \max\left(\min\left(\frac{M^2}{2}\frac{\sqrt{4+(1-M^2)^2}}{1+M^2}, 1\right), \epsilon\right), \tag{2.6}$$

where ϵ is a small threshold value to avoid completely switching off the dissipation. A function that retains the majority of $f_1(M)$ but includes larger Mach number for not very strong shocks is

$$f_2(M) = (Q(M, 2) + Q(M, 3.5))/2 \tag{2.7}$$

or

$$\overline{f_2(M)} = \max((Q(M, 2) + Q(M, 3.5))/2, \epsilon), \tag{2.8}$$

where

$$Q(M, a) = \begin{cases} P(M/a) & M < a \\ 1 & \text{otherwise} \end{cases}. \tag{2.9}$$

The polynomial

$$P(x) = x^4(35 - 84x + 70x^2 - 20x^3) \tag{2.10}$$

is monotonically increasing from $P(0) = 0$ to $P(1) = 1$ and has the property that $P'(x)$ has three continuous derivatives at $x = 0$ and at $x = 1$.

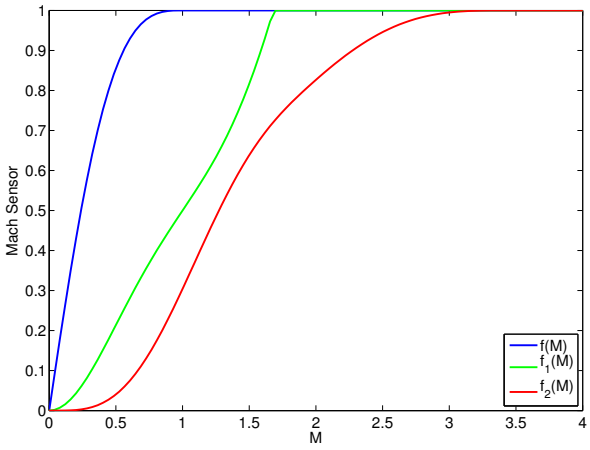

FIGURE 1. Mach sensors: original function f of Li and Gu and its modifications f_1 and f_2

For subsonic speeds a simple and efficient global $\overline{\kappa}$ can be obtained according to the maximum Mach number of the entire flow field and the value is determined by $f_1(M)$ or $f_2(M)$ for non-zero $\omega^l_{j+1/2}$. It is noted that if the original $f(M)$ were used instead of $f_1(M)$ or $f_2(M)$ in Eq.(2.4), the amount of nonlinear filter dissipation could be too large for very low speed turbulent flows (for the same fixed κ). See Figure 1 for details.

2.3. *Local flow sensor for a wide spectrum of flow speed and shock strength*

At each time step and grid point, the aforementioned global $\overline{\kappa}$ is not sufficient to reduce the amount of numerical dissipation where needed for flows that contain a variety of flow features. A more appropriate approach is to obtain a local κ that is determined similar to $\overline{\kappa}$ at each grid point. If known, a dominating shock jump variable should be used for shock detections. In other words, the filter numerical flux indicated in Eq.(2.3) is replaced by:

$$\overline{h}^l_{j+1/2} = \frac{1}{2}[\kappa^l_{j+1/2}\omega^l_{j+1/2}\phi^l_{j+1/2}]. \tag{2.11}$$

In this formula all the variables are supposed to be evaluated at the Roe-average state. However, the results presented in this paper are obtained with simple averaging for local $\kappa^l_{j+1/2}$, i.e. $\kappa_{j+1/2} = (\kappa_j + \kappa_{j+1})/2$ for efficiency. However, this approach was not sufficient for the case with isotropic turbulence, where we use $\kappa_{j+1/2} = \max(\kappa_j, \kappa_{j+1})$ over all 3 directions.

In the case of unknown physics and without experimental data or theory for comparison, $\kappa^l_{j+1/2}$ has to depend on the local Mach number in low speed or smooth flow regions, and on local shock strength in shock regions and turbulent fluctuations in vortical regions in order to minimize the tuning of parameters. According to the local flow type, for each non-zero wavelet indicator $\omega^l_{j+1/2}$, $\kappa^l_{j+1/2}$ should provide the aforementioned amount (between $[0,\ 1]$) to be filtered by the shock-capturing dissipation $\phi^l_{j+1/2}$. For problems containing turbulence and strong shocks, the shock strength should come into play. One measure of the shock strength can be based on the numerical Schlieren formula Hadjadj & Kudryavtsev (2005) for the chosen variables that exhibit the strongest shock strength. In the vicinity of turbulent fluctuation locations, $\kappa^l_{j+1/2}$ will be kept to the same order as in the nearly incompressible case, except in the vicinity of high shear and shocklets.

Due to the fact that $\overline{\kappa}$ works well for local Mach number below 0.4, κ only needs to be modified in regions that are above 0.4. In other words, the final value of $\kappa^l_{j+1/2}$ is determined by the previous local $\overline{\kappa}$, if the local Mach number is below 0.4. If the local Mach number is above 0.4, at discontinuities detected by the non-zero wavelet indicator, $\omega^l_{j+1/2}$, $\kappa^l_{j+1/2}$ is determined by the shock strength (normalized between [0, 1]) based on the Schlieren formula near discontinuities. Again, if known, dominating shock jump variables should be used for shock detection.

At locations with turbulence, determined by the turbulent sensor (e.g., $\omega^l_{j+1/2}$ obtained from employing wavelets with higher order vanishing moments), $\kappa^l_{j+1/2}$ is kept to the same order as in the nearly incompressible case, except in the vicinity of high shear and shocklet locations, where a slightly larger $\kappa^l_{j+1/2}$ would be used. Wavelets for detecting turbulent flow can be (a) wavelets with higher order vanishing moments, and (b) wavelet based Coherent Vortex Extraction (CVE) of Farge *et al.* (2001). Since most flow sensors are not optimal for all flow types, other sensors were discussed in Yee & Sjögreen (2009). For example, in a multi scale flow, the best fit local flow sensor would require the switching among (or the combination of) wavelets, (Ducros *et al.* 2000) and gradient sensors (Ducros *et al.* 2000) from region to region of the flow field.

3. Test cases

In this section we illustrate the performance of the high-order filter schemes with different dissipation control parameters on a set of benchmark solutions. The first three problems are inviscid and the last one is viscous. For each test case the results are obtained for on a coarse grid and compared with the reference solution that can be either an analytical approximation or a solution by a standard method on a grid convergence process. Also we compare the performance of the dissipation control using local κ with the one using the global κ. Note that the results obtained by filter methods presented in Johnsen *et al.* (2010) are using constant κ which depending on the choice of the constant may obtain results similar to the case when using global κ technique. Also all test cases include the results obtained by the filter scheme with constant dissipation control for which only values of $\kappa = 1$ and $\kappa = 0.4$ have been picked in order not to complicate the plots.

For comparison with the the standard schemes, WENO of 7^{th} order is used, designated as WENO7. All the filter schemes considered here imply central schemes of 8^{th} order and Ducros splitting filtered with the dissipative portion of WENO7 and designated as WENO7fi+split.

3.1. *Shu-Osher problem*

The first test case we consider is the Shu-Osher problem (Shu & Osher 1989). This is a one-dimensional idealization of shock-turbulence interaction in which a shock propagates into a perturbed density field. The goal of this problem is to test the capability to accurately capture a shock wave, its interaction with an unsteady density field, and the waves propagating downstream of the shock. The one-dimensional Euler equations with $\gamma = 1.4$ are solved on the domain $x \in [-5, 5]$ with $\Delta x = 0.05$ and initial conditions

$$(\rho, u, p) = \begin{cases} (3.857143, 2.629369, 10.33333) & x < -4, \\ (1 + 0.2\sin(5x), 0, 1) & x \geq 4. \end{cases} \tag{3.1}$$

This problem corresponds to a $M = 3$ shock moving into a field with a small density

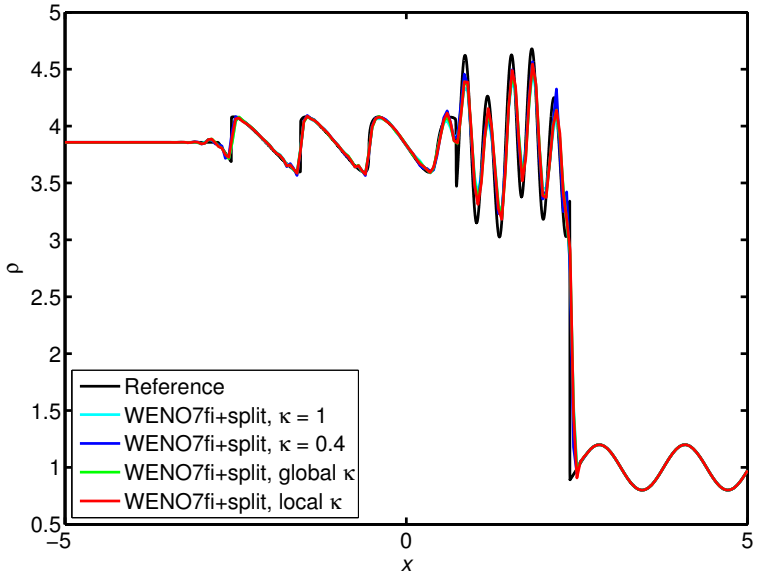

FIGURE 2. Density profiles for the Shu-Osher problem with $\Delta x = 0.05$ and $t = 1.8$. Comparison of WENO7fi+split with a different control of dissipation amount. Reference solution is with $\Delta x = 6.25 \times 10^{-4}$.

(or entropy) disturbance. The solution is compared to a reference solution with $\Delta x = 6.25 \times 10^{-4}$.

The density and velocity profiles at time $t = 1.8$ are shown on Figs 2 and 3. The interaction between the shock and the entropy disturbance generates both acoustic and entropy waves downstream of the shock. The acoustic waves are strong enough to steepen into weak shock waves. At the given time, the shock location is $x_s \approx 2.39$, the location of the contact discontinuity at the leading entropy wave is $x_c \approx 0.69$, and the location of the leading acoustic wave is $x_a \approx 2.75$.

For this test case the results obtained by the scheme using $\kappa = 0.4$ contain spurious oscillations because of too small dissipation. On the contrary, the results obtained by regular WENO7 are too dissipative. The results of all the other schemes are close to each other and in better agreement with the reference solution. The scheme with local κ obtains a little more dissipative but a little less oscillatory results than the schemes with global κ and $\kappa = 1$. Note that when $\kappa = 1$, the full amount of the shock-capturing numerical dissipation is being employed.

3.2. *Shock-vorticity/entropy wave interaction*

A generalization of the Shu-Osher problem is the two-dimensional interaction of a vorticity/entropy wave with a normal shock (Mahesh 2000). The two-dimensional Euler equations are solved with $\gamma = 1.4$ on the domain $x \in [0, 4\pi], y \in [-\pi, \pi)$ with $\Delta x = \pi/50, \Delta y = \pi/16$. Periodic boundaries are used in the y-direction; $x = 0$ is a supersonic inflow, and $x = 4\pi$ is a subsonic outflow. Different techniques are employed to avoid acoustic reflections from the outflow, including an extension of the domain with a sponge region. First a one-dimensional base solution corresponding to a $M = 1.5$ shock is defined

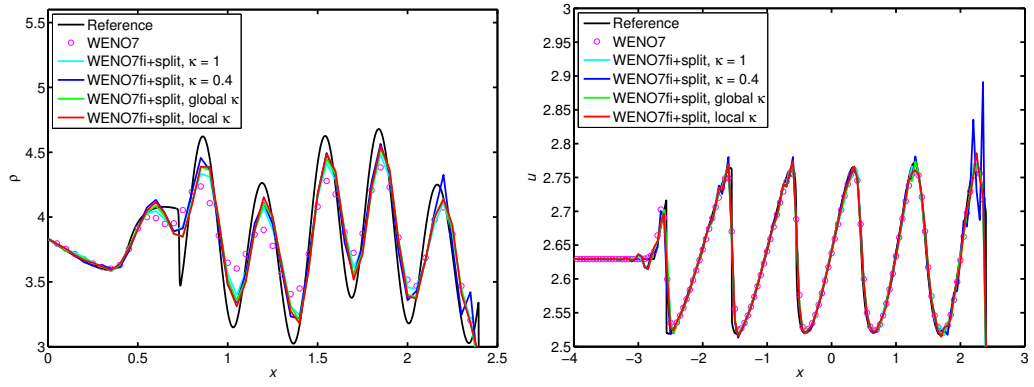

(a) (b)

FIGURE 3. Zoom of density (a) and velocity (b) profiles for the Shu-Osher problem with $\Delta x = 0.05$ and $t = 1.8$. Comparison of WENO7fi+split with a different control of dissipation amount. Reference solution is with $\Delta x = 6.25 \times 10^{-4}$.

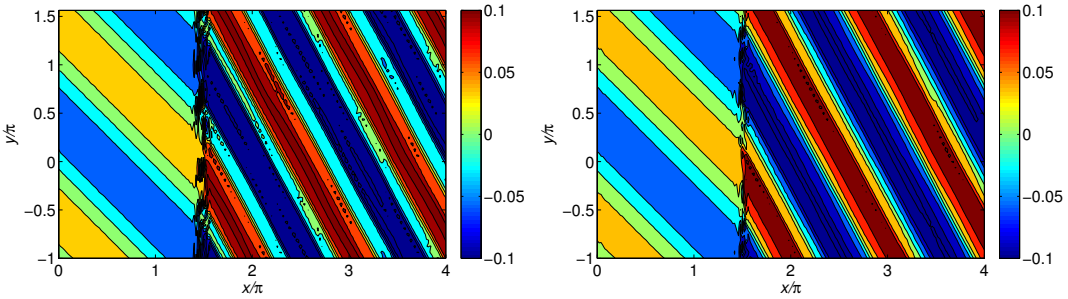

(a) (b)

FIGURE 4. Instantaneous vorticity contours for the shock-vorticity/entropy wave interaction at $t = 25$ obtained by WENO7fi+split: (a) global dissipation control, (b) local dissipation control.

as

$$(\bar{\rho}, \bar{u}_x, \bar{p}) = \begin{cases} (\rho_L, u_L, p_L) = (1, 1.5, 0.714286), & x < 3\pi/2, \\ (\rho_R, u_R, p_R) = (1 + 0.2\sin(5x), 0, 1), & x \geq 3\pi/2. \end{cases} \tag{3.2}$$

A combined vorticity/entropy wave is superposed onto the base flow. The initial data then becomes

$$\begin{aligned} \rho &= \bar{\rho} + \rho_L A_e \cos(k_x x + k_y y), \\ u_x &= \bar{u}_x + u_L A_v \sin\psi \cos(k_x x + k_y y), \\ u_y &= -u_L A_v \cos\psi \cos(k_x x + k_y y), \\ p &= \bar{p}. \end{aligned} \tag{3.3}$$

The conditions at the inflow boundary $x = 0$ are:

$$\begin{aligned} \rho &= \rho_L + \rho_L A_e \cos(k_y y - k_x u_L t), \\ u_x &= u_L + u_L A_v \sin\psi \cos(k_y y - k_x u_L t), \\ u_y &= -u_L A_v \cos\psi \cos(k_y y - k_x u_L t), \\ p &= p_L. \end{aligned} \tag{3.4}$$

For the present study, $k_x = 1/\tan\psi, \psi = 45°, k_y = 1, A_e = A_v = 0.025$.

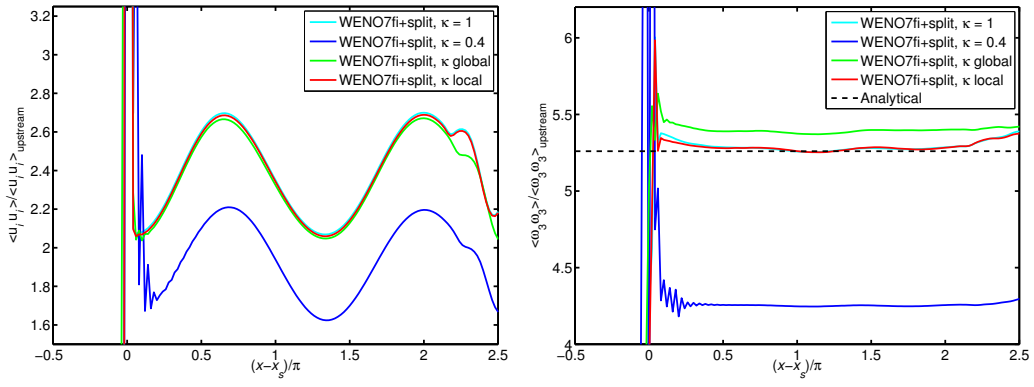

(a) (b)

FIGURE 5. Kinetic energy profiles (a) and mean-square vorticity (b) for the shock-vorticity/entropy wave interaction averaged in a span and time period, obtained by WENO7fi+split with different control of dissipation amount. The analytical solution is the linear analysis of Mahesh (2000).

Figure 4 shows instantaneous vorticity contours obtained by schemes with global and local dissipation control. The results obtained with local κ have fewer oscillations especially in the vicinity of the shock. Figure 5 shows kinetic energy profiles and mean-square vorticity profiles averaged in span and time period obtained by different methods. The vorticity profiles are compared with the linear analysis of Mahesh (2000). All methods show oscillatory behavior near the shock. The case with $\kappa = 0.4$ has the highest oscillations. For this case only methods with local κ and with $\kappa = 1$ obtain vorticity close to analytical level. The method with global κ overestimates vorticity, and the method with $\kappa = 0.4$ underestimates it. The reason why global κ control shows poorer results for this case might be connected with using the Mach curve 2.7 for the whole range of M, whereas local κ algorithm implies using it only for $M < 0.4$ and computing shock strength using Schlieren formula.

3.3. *Taylor-Green vortex*

From a well-resolved initial condition, the inviscid Taylor-Green vortex (Taylor & Green 1937) begins stretching and producing ever smaller scales. It thus constitutes a non-regularized problem with no lower bound on the length scale and is solved with no regularization other than that provided by the numerical method. The goal of this problem is to provide a test of the stability of the methods for severely under-resolved motions, as well as a measure of the preservation of kinetic energy and the growth of enstrophy. The three-dimensional Euler equations are solved with gas constant $\gamma = 5/3$. The domain is a cube with edge length 2π and the grid size is 64^3. Boundary conditions are periodic in all directions. The initial conditions are

$$\begin{aligned} &\rho = 1, \\ &u_x = \sin x \cos y \cos z, \\ &u_y = -\cos x \sin y \cos z, \\ &u_z = 0, \\ &p = 100 + ([\cos(2z) + 2][\cos(2x) + \cos(2y)] - 2)/16, \end{aligned} \tag{3.5}$$

where the mean pressure is sufficiently high to make the problem essentially incompressible. In the 3D inviscid problem the kinetic energy should remain constant while the

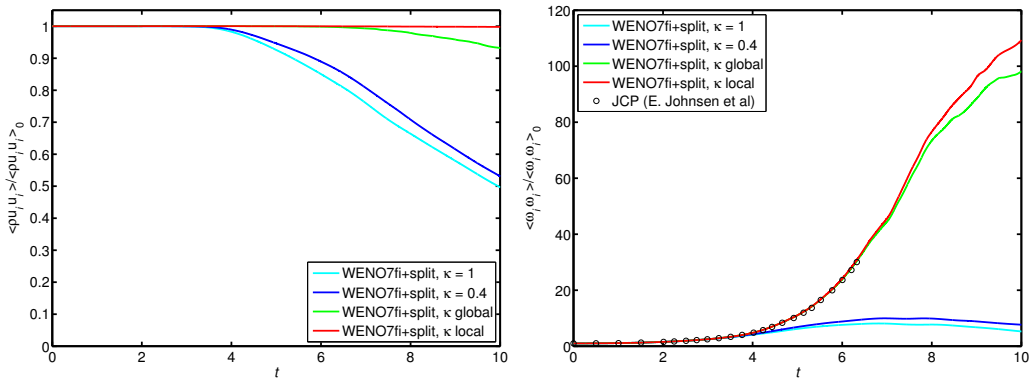

(a) (b)

FIGURE 6. Kinetic energy (a) and enstrophy (b) for the Taylor-Green vortex problem obtained by WENO7fi+split with different control of dissipation amount. The enstrophy is also compared with the results from Johnsen *et al.* (2010) obtained by *Hybrid* code.

enstrophy grows rapidly. Figure 6 shows the results obtained by different methods. The left part of Figure 6 represents the kinetic energy time evolution averaged by the computational domain. The kinetic energy is conserved only in the case of using local κ. The rest of the methods are not able to conserve kinetic energy, although the method with global κ has much smaller loss of energy than methods with $\kappa = \text{const}$. The right part of Figure 6 represents enstrophy evolution obtained by filter schemes and *Hybrid* code from Johnsen *et al.* (2010). Inside the range $t \in [0; 6.5]$ where we have data to compare with Johnsen *et al.* (2010), both methods with global and local dissipation control agree to the results obtained by *Hybrid* code. Both methods with $\kappa = 1$ and $\kappa = 0.4$ essentially underestimate the growth of the enstrophy.

3.4. *Compressible isotropic turbulence*

The final test case is that of decaying compressible isotropic turbulence with eddy shocklets (Lee *et al.* 1991). Given a sufficiently high turbulent Mach number M_t , weak shock waves (eddy shocklets) develop spontaneously from the turbulent motions. The goal of this problem is to test the ability of the methods to handle shocklets when locations are not known a priori, as well as the accuracy for broadband motions in the presence of shocks. The three-dimensional Navier-Stokes equations with $\gamma = 1.4$ are solved on the cube with the edge size 2π, grid size 64^3 and periodic boundary conditions in all directions. The physical viscosity is assumed to follow a power-law of the type:

$$\mu/\mu_{ref} = (T/T_{ref})^{3/4}. \tag{3.6}$$

The initial condition consists of a random solenoidal velocity field $u_{i,0}$ that satisfies

$$E(k) \sim k^4 \exp(-2(k/k_0)^2), \quad \frac{3}{2}u_{rms,0}^2 = \frac{\langle u_{i,0}u_{i,0}\rangle}{2} = \int_0^\infty E(k)dk. \tag{3.7}$$

The brackets here denote averaging over the entire computational domain. For this study, in order to be consistent with Johnsen *et al.* (2010), we chose $u_{rms,0} = 1$ and $k_0 = 4$. The density and pressure fields are initially constant with initial turbulent Mach number $M_{t,0} = 0.6$ and Taylor-scale Reynolds $Re_{\lambda,0} = 100$. These parameters are defined as

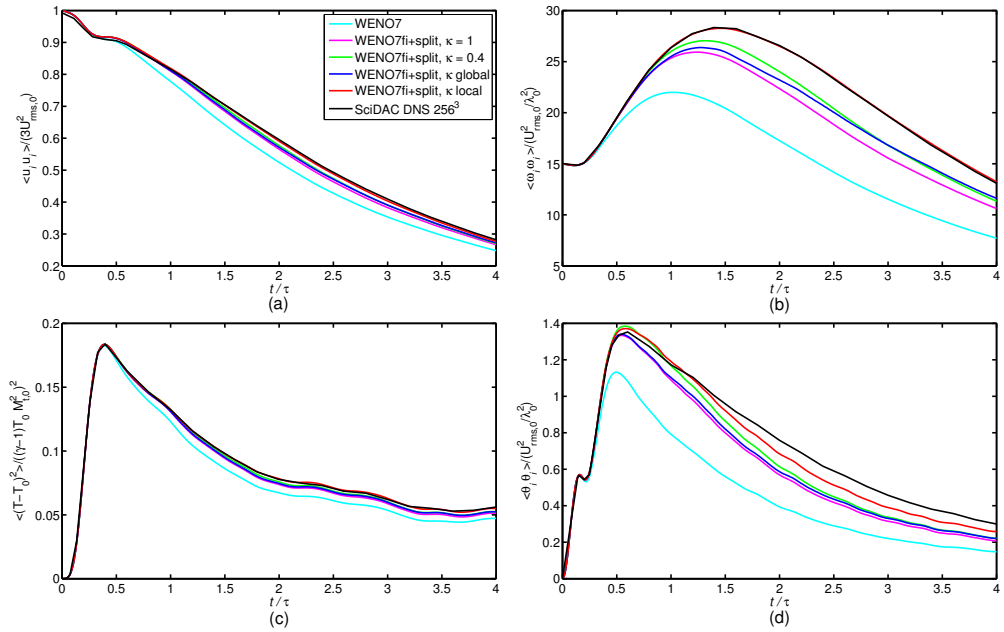

FIGURE 7. Temporal evolution of the variance of different quantities for the isotropic turbulence problem on 64^3 grid: (a) kinetic energy, (b) enstrophy, (c) temperature variance, (d) dilatation, $\theta_i = \partial_i u_i$. The reference is the solution from Johnsen *et al.* (2010) on a 256^3 grid spectrally filtered to a 64^3 grid.

follows:

$$M_t = \frac{\sqrt{\langle u_i u_i \rangle}}{\langle c \rangle}, \quad Re_\lambda = \frac{\langle \rho \rangle \, u_{rms} \lambda}{\langle \mu \rangle}, u_{rms} = \sqrt{\frac{\langle u_i u_i \rangle}{3}}, \quad \lambda = \sqrt{\frac{\langle u_x^2 \rangle}{\langle (\partial_x u_x)^2 \rangle}}. \tag{3.8}$$

The time scale is $\tau = \lambda_0 / u_{rms,0}$ and the final time is $t/\tau = 4$.

The temporal evolution of the mean-square velocity and vorticity and the temperature variance and dilatation are shown on Figure 7. The reference solution is the solution from Johnsen *et al.* (2010) obtained by DNS on 256^3 grid spectrally filtered to a 64^3 grid. All four methods with dissipation control are much closer to the reference solution than standard WENO7, and all four methods agree quite well with DNS results for mean-square velocity and temperature variance. However, only the method with local κ agrees well with DNS results for vorticity (right-top plot Figure 7). Also this method is the closest one to DNS dilatation results (right bottom plot on Figure 7).

Instantaneous profiles of dilatation, density, temperature variance and vorticity through an eddy shocklet are shown in Figure 8. The shocklet is located at $x \approx 2.8$, i.e., at the point of large negative dilatation. All methods show reasonable results for a coarse grid such as 64^3 and, as expected, none could resolve the shocklet. The biggest discrepancy from DNS results is obtained by regular WENO7. The other four methods obtained similar results. The method with local κ obtains results slightly closer to the reference than the other methods.

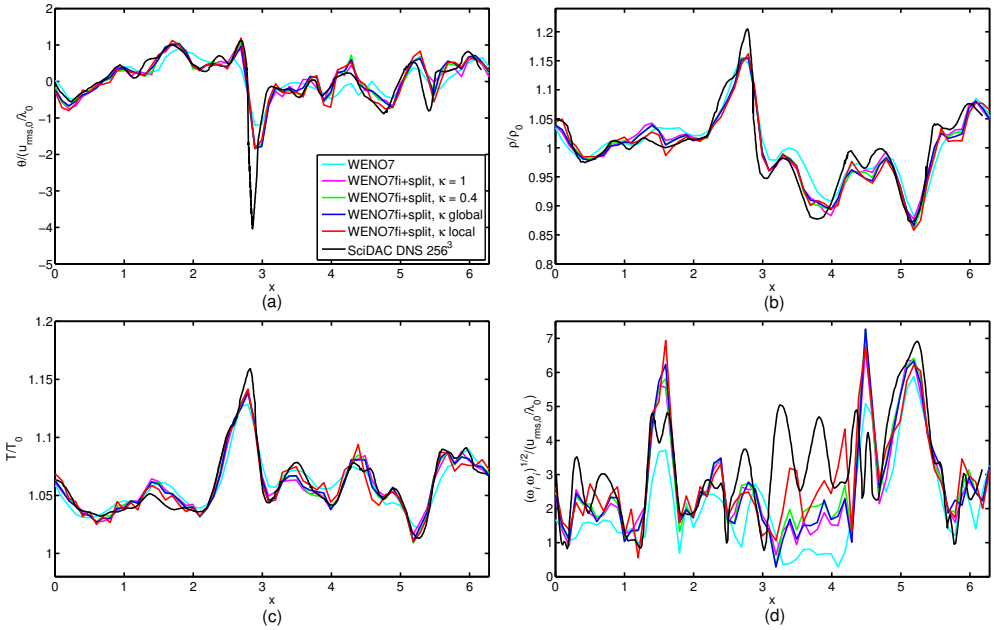

FIGURE 8. Instantaneous profiles through a shocklet (at $x \approx 2.8$) for the isotropic turbulence problem on 64^3 grid at $t/\tau = 4$: (a) kinetic energy, (b) enstrophy, (c) temperature variance, (d) dilatation, $\theta_i = \partial_i u_i$. The reference is the solution from Johnsen *et al.* (2010) on a 256^3 grid spectrally filtered to a 64^3 grid.

4. Conclusions

The performance of the filter scheme with improved dissipation control κ has been demonstrated for different flow types. The scheme with local κ is shown to obtain more accurate results than its counterparts with global or constant κ. At the same time no additional tuning is needed to achieve high accuracy of the method when using the local κ technique. However, further improvement of the method might be needed for even more complex and/or extreme flows.

Acknowledgments

The support of the DOE/SciDAC SAP grant DE-AI02-06ER25796 is acknowledged.

REFERENCES

DUCROS, F., LAPORTE, F., SOULÈRES, T., GUINOT, V., MOINAT, P. & CARUELLE, B. 2000 High-order fluxes for conservative skew-symmetric-like schemes in structured meshes: Application to compressible flows. *J. Comput. Phys.* **161**, 114–139.

FARGE, M., PELLEGRINO, G. & SCHNEIDER, K. 2001 Coherent vortex extraction in 3d turbulent flows using orthogonal wavelets. *Phys. Rev. Lett.* **5**, 45011–45014.

HADJADJ, A. & KUDRYAVTSEV, A. 2005 Computation and flow visualization in high speed aerodynamics. *J. Turbul.* **6**, 33–81.

JOHNSEN, E., LARSSON, J., BHAGATWALA, A., CABOT, W., MOIN, P., OLSON, B., RAWAT, P., SHANKAR, S., SJGREEN, B., YEE, H., ZHONG, X. & LELE, S. 2010

Assessment of high-resolution methods for numerical simulations of compressible turbulence with shock waves. *J. Comput. Phys.* **229**, 1213–1237.

Lee, S., Lele, S. & Moin, P. 1991 Eddy shocklets in decaying compressible turbulence. *Phys. Fluids* **3**, 657–664.

Li, X.-S. & Gu, C.-W. 2008 An all-speed roe-type scheme and its asymptotic analysis of low mach number behaviour. *J. Comp. Phys.* **227**, 5144–5159.

Mahesh, K. 2000 The interaction of a shock wave with a turbulent shear flow. PhD thesis, Stanford University.

Olsson, P. 1995 Summation by parts, projections, and stability. I. *Math. Comp.* **64**, 1035–1065.

Olsson, P. & Oliger, J. 1994 Energy and maximum norm estimates for nonlinear conservation laws. *Tech. Rep.* 94.01. RIACS.

Shu, C.-W. & Osher, S. 1989 Efficient implementation of essentially non-oscillatory shock-capturing schemes, II. *J. Comp. Phys.* **83**, 32–78.

Sjögreen, B. & Yee, H. 2007 On tenth-order central spatial schemes. In *Proceedings of the Turbulence and Shear Flow Phenomena 5 (TSFP-5)*. Munich, Germany.

Sjögreen, B. & Yee, H. C. 2004 Multiresolution wavelet based adaptive numerical dissipation control for shock-turbulence computation. *J. Sci. Comput.* **20**, 211–255.

Sjögreen, B. & Yee, H. C. 2009 On skew-symmetric splitting and entropy conservation schemes for the euler equations. In *Proc. of the 8th Euro. Conf. on Numerical Mathematics & Advanced Applications (ENUMATH 2009)*. Uppsala University, Uppsala, Sweden.

Taylor, G. & Green, A. 1937 Mechanism of the production of small eddies from large ones. *Proc. R. Soc. London* **A 158**, 499–521.

Vinokur, M. & Yee, H. 2002 Extension of efficient low dissipative high-order schemes for 3D curvilinear moving grids. *Frontiers of Computational Fluid dynamics, World Scientific* pp. 129–164.

Yee, H. & Sjögreen, B. 2002 Designing adaptive low dissipative high order schemes for long-time integrations. In *Turbulent Flow Computation* (ed. D. D. . B. Geurts). Kluwer Academic.

Yee, H. & Sjögreen, B. 2007 Development of low dissipative high order filter schemes for multiscale navier-stokes/MHD systems. *J. Comput. Phys.* **225**, 910–934.

Yee, H., Vinokur, M. & Djomehri, M. 2000 Entropy splitting and numerical dissipation. *J. Comput. Phys.* **162**, 33–81.

Yee, H. C. 2002 Building blocks for reliable complex nonlinear numerical simulations. In *Turbulent Flow Computation* (ed. D. D. . B. Geurts). Kluwer Academic.

Yee, H. C. & Sjögreen, B. 2009 High order filter methods for wide range of compressible flow speeds. In *Proc. of ICOSAHOM 09 (International Conference on Spectral and High Order Methods)*. Trondheim, Norway.

Yee, H. C. & Sweby, P. 1997 Dynamics of numerics & spurious behaviors in CFD computations. In *Keynote paper, 7th ISCFD Conf.*. Beijing, China, rIACS Technical Report 97.06, June 1997.

Yee, H. C., Torczynski, J., Morton, S., Visbal, M. & Sweby, P. 1999 On spurious behavior of CFD simulations. *Int. J. Num. Meth. Fluids* **30**, 675–711.